JOURNAL OF SOLID STATE CHEMISTRY 60, 320–331 (1985)

Microdomains in the Reduction of $Ca_2LaFe_3O_{8+z}$

J. M. GONZÁLEZ-CALBET, M. VALLET-REGÍ,
AND M. A. ALARIO-FRANCO*

Departamento de Química Inorgánica, Facultad de Ciencias Químicas, Universidad Complutense, 28040 Madrid, Spain

Received February 21, 1985; in revised form May 31, 1985

The reduction of $Ca_2LaFe_3O_{8+z}$ in the electron microscope shows this solid to decompose into $Ca_2Fe_2O_5$ and $LaFeO_3$, two perovskite-related line-phases which, under these conditions, appear to be thermodynamically more stable. In kinetic terms, the decomposition appears to be of the nucleation and growth type. *Microdomains* appear to be an essential characteristic of the system since they are present in both the reactants and the reaction products. Up to nine sets of structurally-related microdomains can simultaneously be present within the same crystal. This leads to quite elaborate electron diffraction patterns which can be interpreted in terms of perovskite superstructures. These results are discussed in terms of diffusion data on perovskite-like ferrites.

Introduction

In a series of previous papers (*1–4*), we have been dealing with compositional variations and nonstoichiometry in the $Ca_xLa_{1-x}FeO_{3-y}$ system. By means of electron microscopy and diffraction, we have been able to show (*4*) that for the iron(III) case only an intermediate composition exists; this corresponds to $x = \frac{2}{3}$ and $y = x/2$, i.e., $Ca_2LaFe_3O_8$ as shown by Grenier *et al.* (*5*). These authors concluded that the structure of this phase is intermediate between the structures of the end members of the system, namely $LaFeO_3$ (for $x = 0$) and $Ca_2Fe_2O_5$ ($x = 1$), whose structures are described in Refs. (*6*, *7*).

Although the crystal structure of $Ca_2LaFe_3O_8$ is not yet known, a recent HREM study (*2*) confirmed the previous model, according to which a sequence of two octahedra "layers" and one tetrahedra layer follow each other along the c axis of the unit cell (Fig. 1b). All the three phases are, on the other hand, superstructures of the perovskite structure and derive from it by means of compositional and/or structural changes. Figure 1 shows a schematic projection of the three structures.

Perhaps the most striking characteristic of $Ca_2LaFe_3O_8$ is its oxidation process which can be described by

$$Ca_2LaFe_3O_8 + \frac{z}{2}O_2 \xrightarrow{\text{air}} Ca_2LaFe_3O_{8+z} \quad (1)$$

where $z = 0.235$ at 1400°C and is accompanied by the formation of a microdomain texture (Fig. 2). As already discussed (*1*), the structure within each domain is closely related to, but of higher symmetry than, the $Ca_2LaFe_3O_8$ orthorhombic structure. In view of the peculiar character of this oxidation process, it is of obvious interest to

* To whom all correspondence should be addressed.

0022-4596/85 $3.00

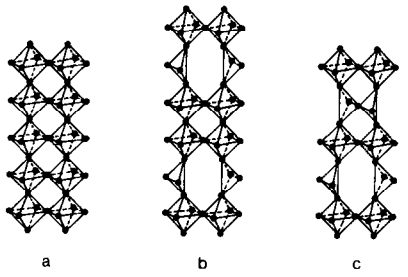

FIG. 1. Schematic representation of (a) $LaFeO_3$, (b) $Ca_2LaFe_3O_8$, and (c) $Ca_2Fe_2O_5$ structures along $[110]_c$. Subscript c refers to the simple cubic pervoskite cell.

study the reduction of $Ca_2LaFe_3O_{8+z}$. We describe and discuss in the following the result of such a study.

Experimental

Samples of $Ca_2LaFe_3O_{8+z}$ were prepared by J. C. Grenier. Full details are given in Ref. (*1*).

Electron diffraction and microscopy was performed on a Siemens Elmiskop 102 electron microscope fitted with a ±45° tilt goniometer stage. Samples were ultrasonically dispersed in *n*-butanol and then transferred to carbon-coated copper grids. Focusing conditions close to the optimum defocus (Scherzer) conditions were employed (*8*).

Results and Discussion

As indicated in the introduction, $Ca_2LaFe_3O_8$ oxidizes in air at high temperature, $T \simeq 1400°C$, in a process in which a microdomain texture is formed. Figures 2a and b show, respectively, an electron diffraction pattern and an electron micrograph of one such sample in the $[001]_c$ subcell orientation. The microdomain texture evident on the micrograph is reflected in the diffraction pattern by three juxtaposed reciprocal lattices corresponding to the three sets of microdomains. The vertical threefold perovskite superlattice in this figure belongs to the set with cell $a_c\sqrt{2} \times 3a_c \times a_c\sqrt{2}$, the horizontal one to the microdomain set with unit cell $3a_c \times a_c\sqrt{2} \times a_c\sqrt{2}$ and the third one corresponding to the domain set having the threefold multiple axis perpendicular to the plane of the pattern (see Ref. (*1*) for details).

This solid, which according to Eq. (1) is a mixed Fe(III)–Fe(IV) phase, appears to be a metastable high-temperature quenched phase. When left at room temperature for long periods of time, of the order of 3 months, the HT phase reverts to $Ca_2LaFe_3O_8$.

Figure 3 shows an electron micrograph of a crystal in an intermediate situation, i.e., a

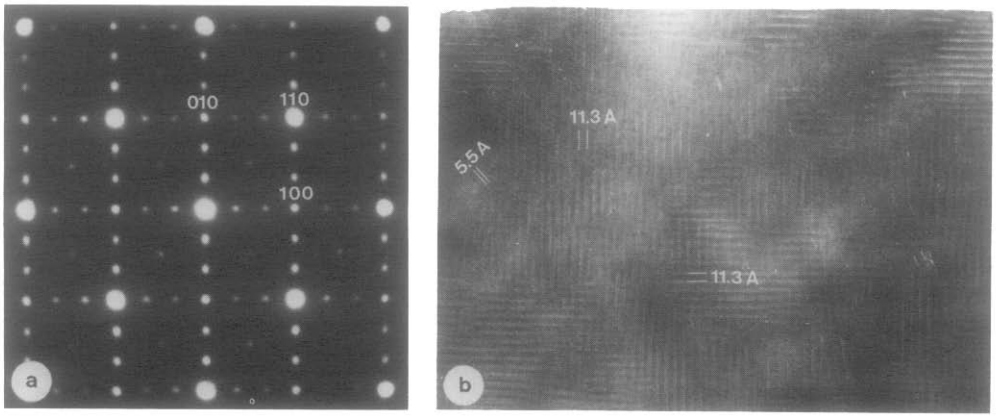

FIG. 2. (a) Electron diffraction pattern of the high-temperature $Ca_2LaFe_3O_{8+z}$ sample along the $[001]_c$ axis. (b) Electron micrograph of this oxidized sample along the same orientation.

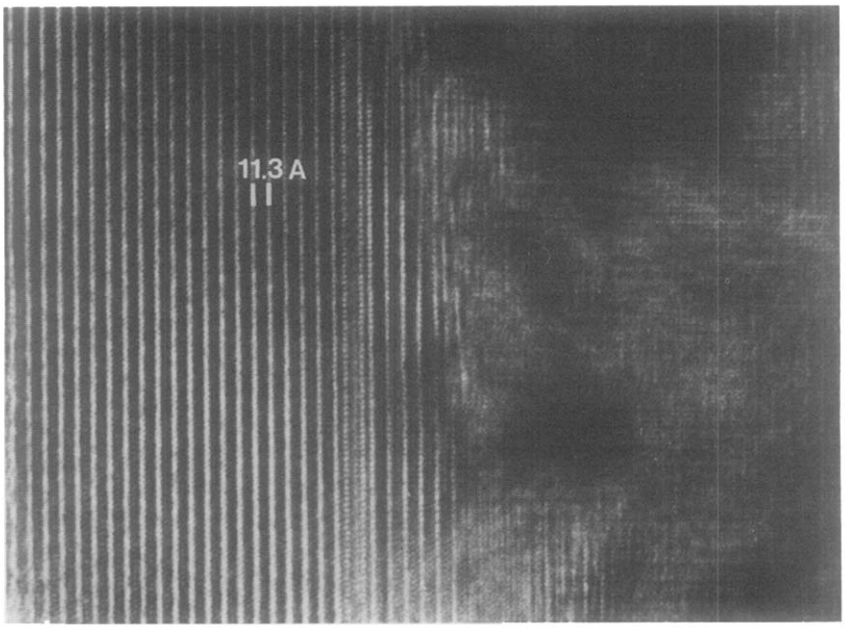

FIG. 3. Electron micrograph of a crystal showing an intergrowth between the reduced (to the left) and the oxidized solids.

"mixed crystal," with $z < 0.235$, but difficult to know precisely for just one microscopic crystal. The left part of the image corresponds to the ordered iron(III) phase, while the right part belongs to an oxidized, i.e., Fe^{III}–Fe^{IV} phase "disordered" in microdomains. An extended defect is also apparent near the border between the two crystal regions. It is really remarkable that the oxygen excess is situated in just one part of the crystal—that showing the microdomains—and not distributed homogeneously, i.e., randomly all over it.

When the $Ca_2LaFe_3O_{8.235}$ sample is left for a few minutes within the microscope under normal observation conditions it becomes reduced by the combined influence of both high vacuum ($\sim 10^{-6}$ Torr) and the electron beam. Although this process is difficult to control, the observations that we have been able to make allow us to describe it.

At first, the electron micrograph still shows domains (Fig. 4a), and the electron diffraction pattern (Fig. 4b) shows two types of diffraction maxima: one, shown schematically in Fig. 4c, is identical to the one shown in Fig. 2a and corresponds to the $Ca_2LaFe_3O_{8+z}$ microdomains. The other type of maxima can be indexed as either a multitwinned $LaFeO_3$ (Fig. 4d (*4*)), a microdomain textured $Ca_2Fe_2O_5$ (Fig. 4e (*3*)), or to both of them, because, in this particular orientation, i.e., $[001]_c$, and in the presence of $Ca_2LaFe_3O_{8+z}$ microdomains, they are indistinguishable. If, in fact, the last interpretation is the correct one, nine sets of microdomains will be present in this crystal. Nevertheless, the subcell reflexions are more intense since in these positions the diffracted intensity from all sets of domains is coincident.

The ease to which this multiple intergrowth can occur is due to the close relationship existing between three structures, all of which are multiples of the perovskite subcell. The differences among them are both compositional and structural (c.f. in-

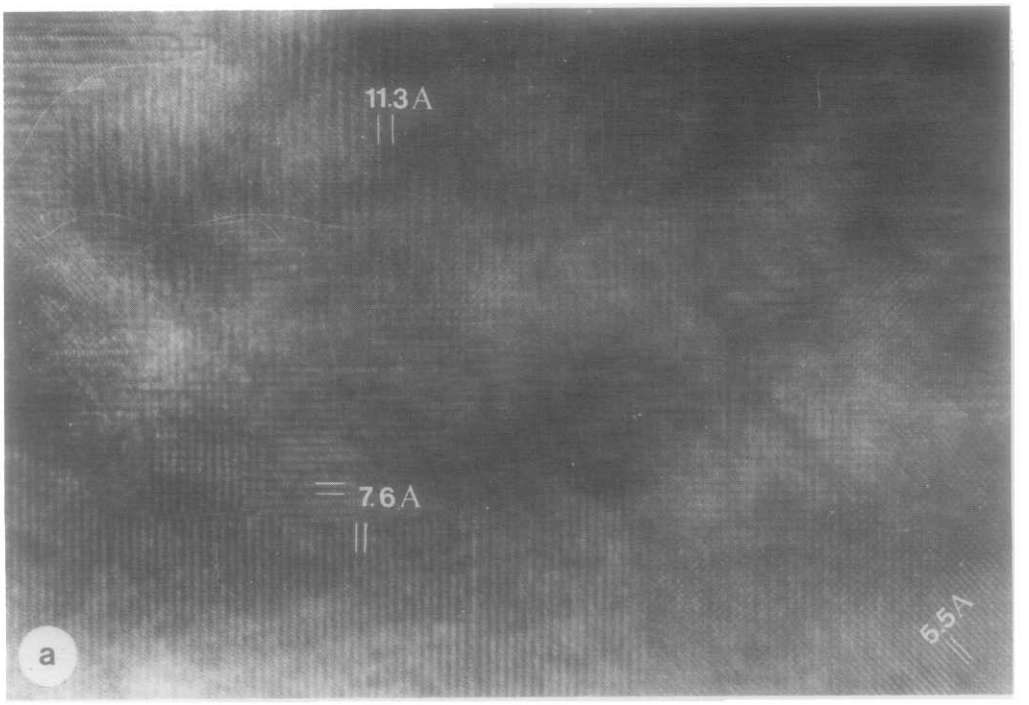

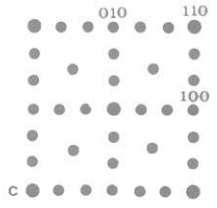

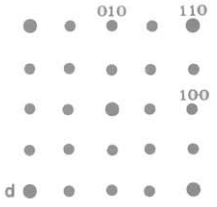

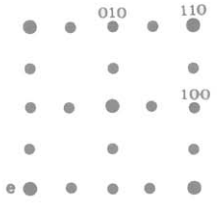

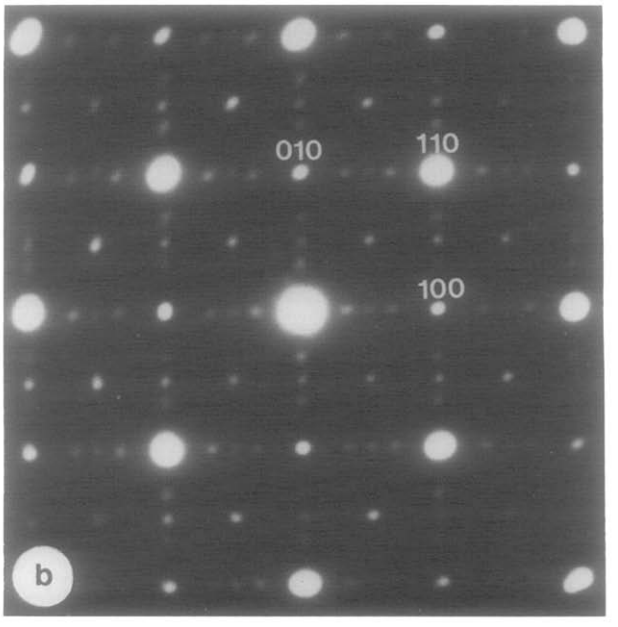

FIG. 4. (a) Electron micrograph of the $Ca_2LaFe_3O_{8+z}$ sample slightly reduced under the electron beam. (b) Electron diffraction pattern along the $[001]_c$ zone-axis of the crystal shown in Fig. 4a. (c) Schematic $[001]_c$ zone-axis electron diffraction pattern of $Ca_2LaFe_3O_{8.235}$. (d) Schematic electron diffraction pattern along $[001]_c$ of a multitwinned $LaFeO_3$. (e) Schematic $[001]_c$ zone-axis electron diffraction pattern of a microdomain textured $Ca_2Fe_2O_5$.

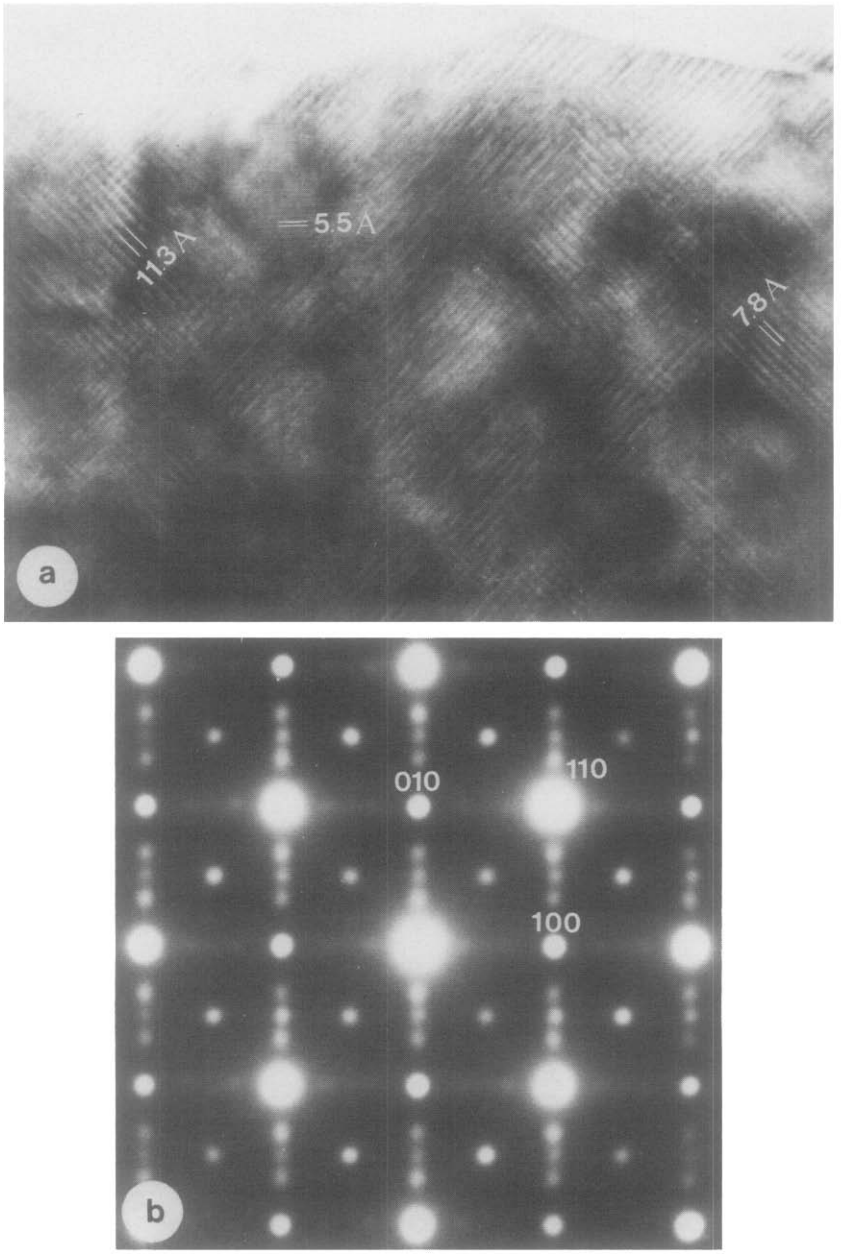

FIG. 5. (a) Electron micrograph of another crystal of the same sample showing smaller domains. (b) Corresponding electron diffraction pattern along the $[001]_c$ zone axis.

TABLE I

UNIT CELL PARAMETERS OF $LaFeO_3$, $Ca_2LaFe_3O_8$ AND $Ca_2Fe_2O_5$

	$LaFeO_3$ (*6*)	$Ca_2LaFe_3O_8$ (*2, 5*)	$Ca_2Fe_2O_5$ (*7*)	Perovskite multiplicity
a (Å)	5.553(2)	5.464(3)	5.4253(5)	$\sim a_c\sqrt{2}$
b (Å)	7.867(3)	11.29(1)	14.7687(17)	$\sim na_c$ (n = 2, 3, 4)
c (Å)	5.563(2)	5.563(3)	5.5980(5)	$\sim a_c\sqrt{2}$

troduction and Refs. *1–4*). Table I recalls the unit cell parameters of the three structures.

The domains seen in Fig. 4a are relatively big; sometimes, however, the resulting domains were much smaller (Fig. 5a). The corresponding electron diffraction pattern (Fig. 5b) can again be interpreted as due to nine sets of domains but from the diffraction intensities it appears that, in this crystal, the domains having the multiple $3a_c$ axis predominate along $[010]_c$. Some streaking, indicative of some disordering, is seen along $[100]_c$.

The apparent misalignment of the superstructure spots along the subcell axes is due to the slight differences in unit cell parameters of the three phases (see Table I).

In yet another set of experiments, Fig. 6, streaks appeared along both a_c^* and b_c^* and, presumably, along c_c^* as well. Apart from the streaks, the pattern on Fig. 6a can be interpreted in the same way as Fig. 4c, i.e., due to the juxtaposition of two or even three sets of domains. The corresponding micrograph, Fig. 6b, shows an extremely disordered crystal with small domains in all possible orientations, i.e.,

$$\left.\begin{aligned} -a_c\sqrt{2} \times a_c\sqrt{2} \times 3a_c&: \text{ set } \alpha \\ -a_c\sqrt{2} \times 3a_c \times a_c\sqrt{2}&: \text{ set } \beta \\ -3a_c \times a_c\sqrt{2} \times a_c\sqrt{2}&: \text{ set } \gamma \end{aligned}\right\} Ca_2LaFe_3O_8$$

$$\left.\begin{aligned} -a_c\sqrt{2} \times a_c\sqrt{2} \times 4a_c&: \text{ set } \delta \\ -a_c\sqrt{2} \times 4a_c \times a_c\sqrt{2}&: \text{ set } \varepsilon \\ -4a_c \times a_c\sqrt{2} \times a_c\sqrt{2}&: \text{ set } \zeta \end{aligned}\right\} Ca_2Fe_2O_5$$

$$\left.\begin{aligned} -a_c\sqrt{2} \times a_c\sqrt{2} \times 2a_c&: \text{ set } \eta \\ -a_c\sqrt{2} \times 2a_c \times a_c\sqrt{2}&: \text{ set } \theta \\ -2a_c \times a_c\sqrt{2} \times a_c\sqrt{2}&: \text{ set } \iota. \end{aligned}\right\} LaFeO_3$$

To these nine sets of domains correspond nine reciprocal lattices whose reciprocal cells are shown in Fig. 7a. On the other hand, Fig. 7b shows the compounded reciprocal unit cell of the whole crystal. A comparison of Figs. 6a and 7b easily explains the origin and intensity of the streaking seen in the former.

However, all the domains having the multiple perovskite axis perpendicular to the image plane, that is, those belonging to sets α, δ, and η are indistinguishable. Also, under these relatively low-resolution conditions and in this orientation $[001]_c$ the brownmillerite images show fringes corresponding to $d_{020} = 7.4$ Å while $LaFeO_3$ is imaged by the $d_{010} = 7.8$ Å and consequently sets ε and ζ are indistinguishable between themselves, apart from their orientation, and cannot be differentiated from sets θ and ι. At the most, then, three different types of domains can be differentiated by their fringe spacing: ~5.5, 7.4 ~ 7.8, and ~11.3 Å; these are shown on Fig. 6b.

Finally, a recrystallization process takes place and the domain size increases. Fig. 8a shows just three domains having very different boundaries: a straight boundary between I and II and a curved boundary between II and III. As the resolution is somewhat better in this picture, Domain I, having its multiple axis perpendicular to the image, is imaged through the perovskite subcell, ~3.9 × 3.9 Å, crossed fringes. Under such an ordered situation streaks have disappeared from the diffraction pattern, Fig. 8b, where the diffraction maxima corresponding to the $Ca_2LaFe_3O_8$ cell have also disappeared. Although with just three sets of domains of a $LaFeO_3$ multitwinned cell all the spots of this pattern can be indexed, —spots at $(0\ \frac{1}{2}\ 0)_c$ belong to set θ, those located at $(\frac{1}{2}\ 0\ 0)_c$ to domain ι and spots at $(\frac{1}{2}\ \frac{1}{2}\ 0)_c$ correspond to domain η —, tilts around a_c^* and b_c^* show patterns which can only be indexed with the juxtaposition of six sets of domains, three from a $Ca_2Fe_2O_5$ brownmillerite-like cell and another three sets belonging to the $LaFeO_3$ cell. In this way, Fig. 9 shows a $[10\bar{1}]_c$ pattern obtained after a tilt of 45° around b_c^*, where the spots located at $(\frac{1}{2}\ \frac{1}{4}\ \frac{1}{2})_c$ and $(\frac{1}{2}\ \frac{3}{4}\ \frac{1}{2})_c$, and equivalent positions, can be indexed on the

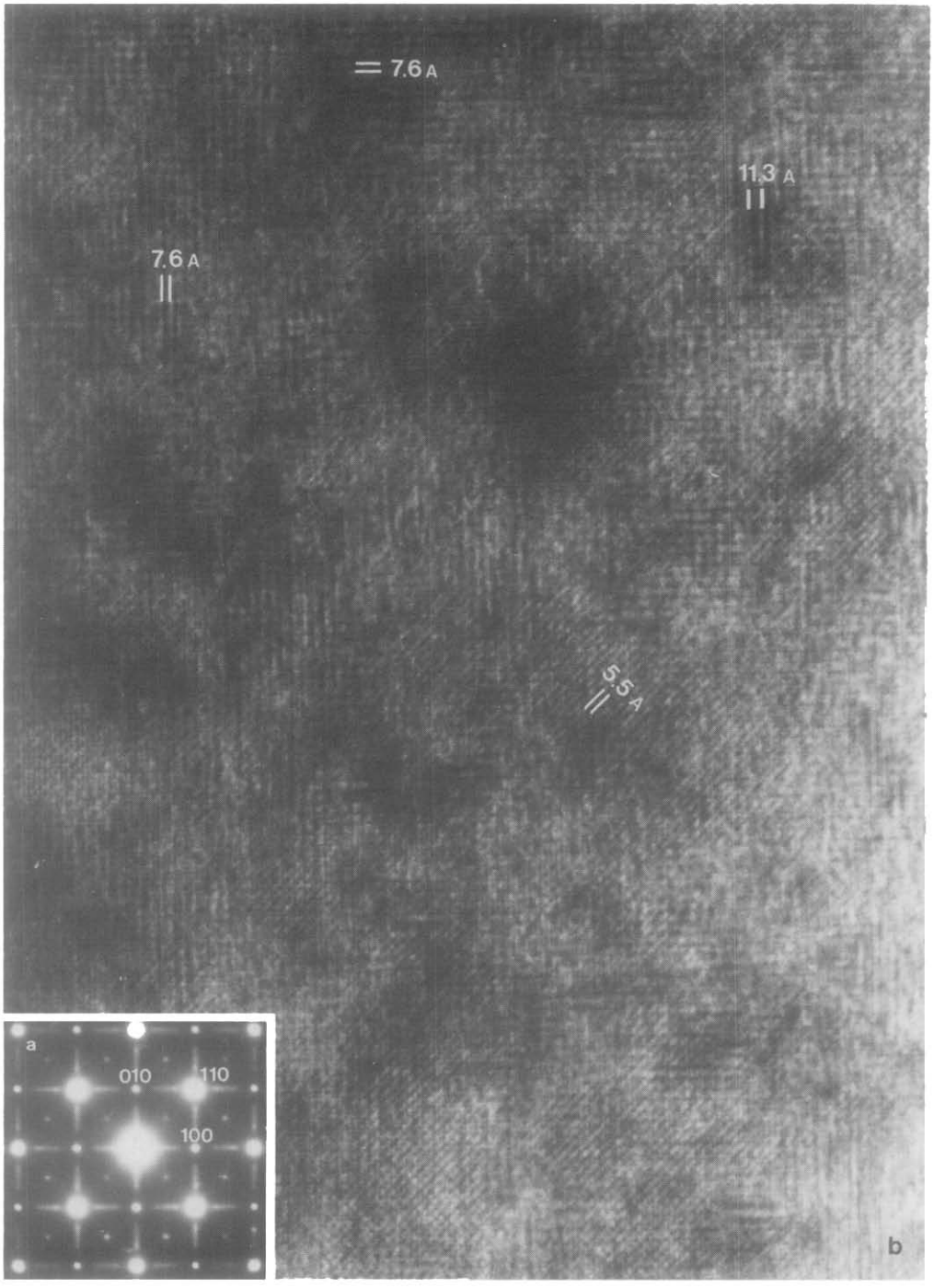

FIG. 6. (a) Electron diffraction pattern along $[001]_c$ of another crystal in a different stage of the reduction process. Streaking along both a_c^* and b_c^* suggest the presence of disorder as shown in the corresponding micrograph (b).

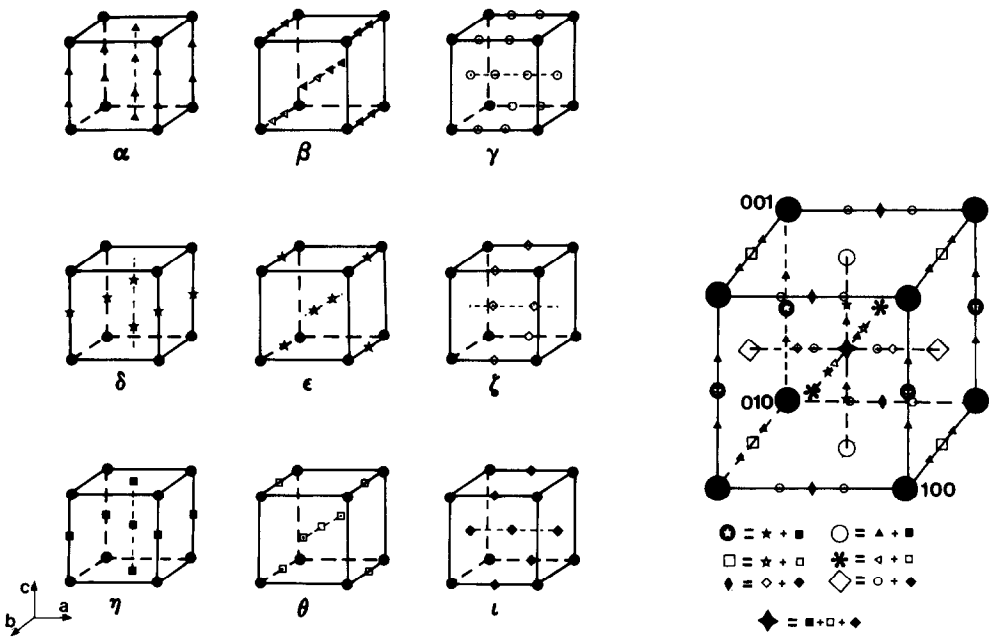

FIG. 7. (a) Schematic reciprocal unit cells of the nine sets of microdomains. (b) Complete reciprocal lattice composed by the juxtaposition of the nine reciprocal nets shown above.

basis of a brownmillerite type cell as shown in domain ε (see Fig. 7). Moreover, if the 45° tilting is performed around a_c^* one obtains an equivalent pattern along $[01\bar{1}]_c$, so that the brownmillerite spots can be represented as in the reciprocal net corresponding to domain ζ.

Figure 10 shows the $[10\bar{2}]_c$ zone axis indexed on the basis of a perovskite cell. Spots appearing at $(\frac{1}{2}\ \frac{1}{2}\ \frac{1}{4})_c$ and $(\frac{3}{2}\ \frac{1}{2}\ \frac{3}{4})_c$, and equivalent positions, correspond to the third brownmillerite net as shown in domain δ.

We can now come back to the chemistry of the problem and, in view of the diffraction evidence described above, it appears that the reduction happens through the process

$$a\mathrm{Ca_2LaFe_3O_{8+z}} \xrightarrow[p\mathrm{O_2} \sim 10^{-5}\ \mathrm{Torr}]{e^-} b\mathrm{Ca_2Fe_2O_5} + b\mathrm{LaFeO_3} + c\mathrm{Ca_2LaFe_3O_{8+z'}} \quad (2)$$

where e^- stands for electrons from the electron beam, $a = b + c$ and when $z' < z$ this situation corresponds to Fig. 4; with yet another value of z and z' it also corresponds to Figs. 5 and 6. These three phases appear textured in microdomains differing in composition and structure between phases but simply related in orientation to each other. Under these highly reducing conditions, when all the oxygen excess is eliminated (i.e., when $z = 0$) no $Ca_2LaFe_3O_8$ is left; it decomposes wholly to $Ca_2Fe_2O_5$ and $LaFeO_3$.

The elimination of oxygen is then accompanied by the decomposition of the phase with $x = \frac{2}{3}$ of the $Ca_xLa_{1-x}FeO_{3-y}$ system into the corresponding end terms having $x = 0$ and $x = 1$, respectively. This process requires the counterdiffusion of calcium and lanthanum ions along the three dimensional framework of A positions characteristic of the perovskite substructure, the same framework that justifies the existence

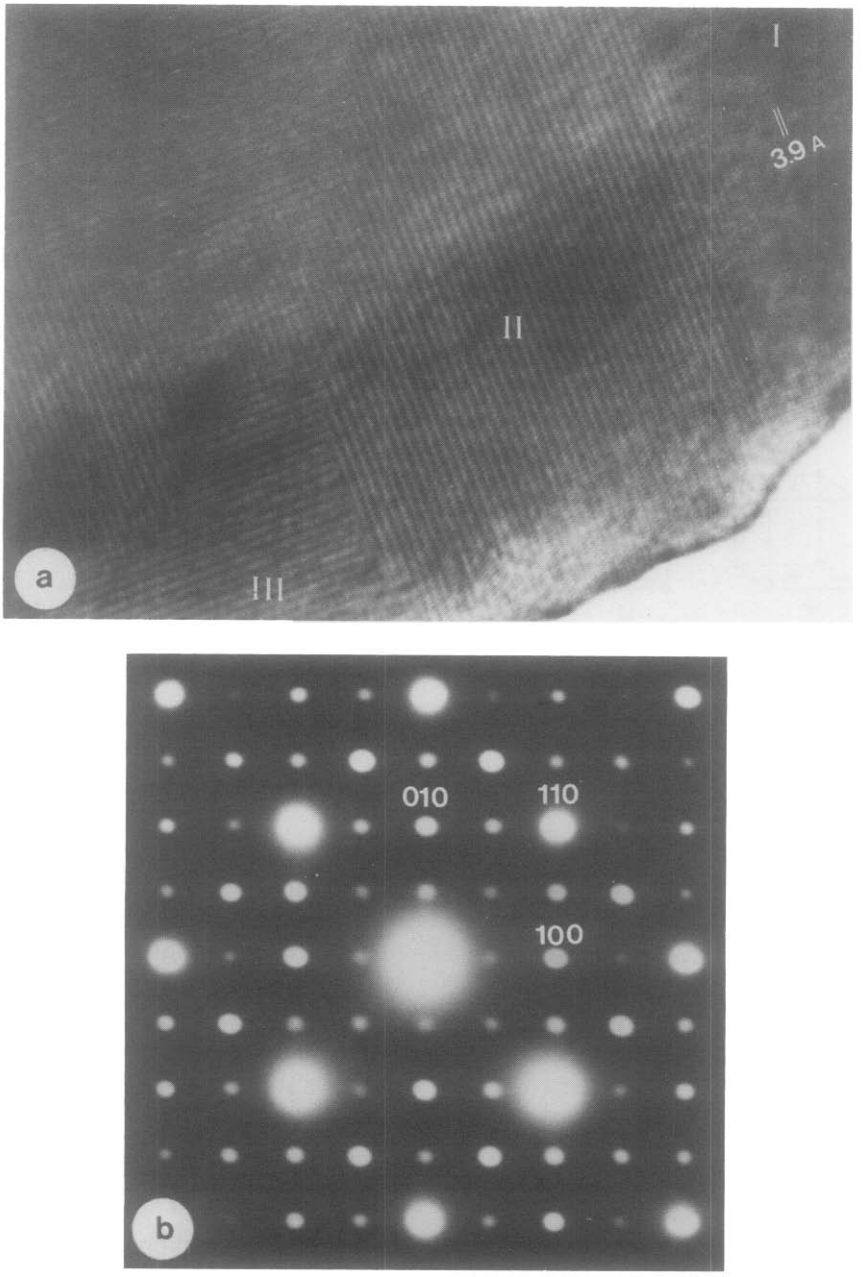

FIG. 8. (a) Electron micrograph of the $Ca_2LaFe_3O_{8+z}$ sample taken when the reduction process under the electron beam is over. (b) Corresponding electron diffraction pattern along $[001]_c$.

and the properties of the well-known bronzes (*9*). Indeed, the oxygen excess given by z in the above formulae does also have to diffuse out of the crystal but this is facilitated by the unoccupied oxygen positions corresponding to the presence of tetrahedra. These form tunnels, parallel to the six $[110]_c$ directions of the perovskite sub-

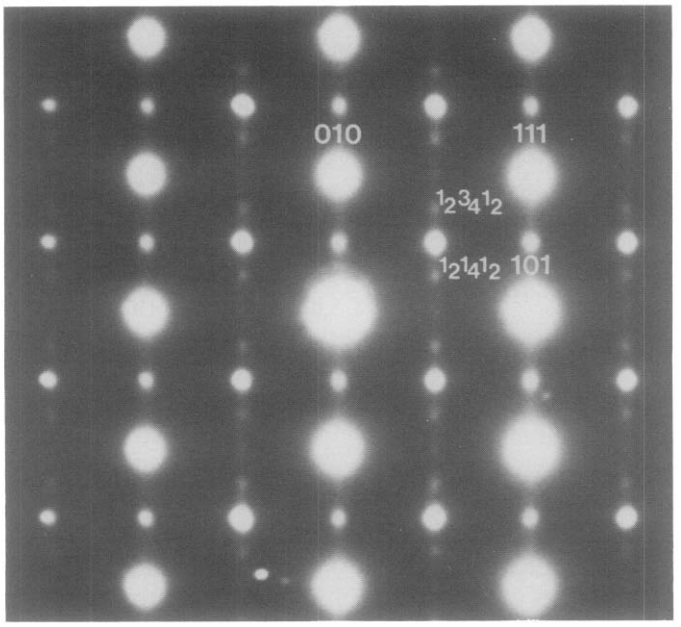

FIG. 9. Electron diffraction pattern along $[10\bar{1}]_c$ of the crystal shown in Fig. 7.

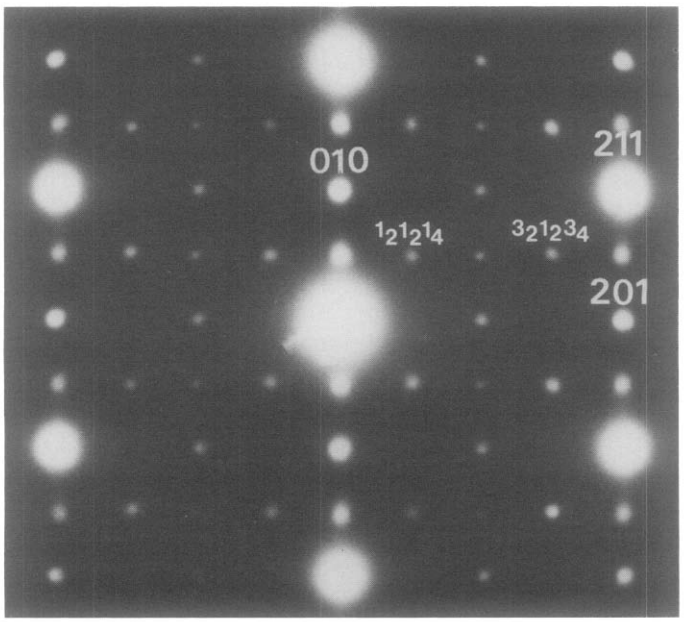

FIG. 10. $[10\bar{2}]_c$ zone-axis electron diffraction pattern of the above crystal.

TABLE II
DIFFUSION COEFFICIENTS OF SOME IONS IN $LaFeO_3$ IN THE TEMPERATURE RANGE 1000–1300°C

Ion	D_0 ($cm^2 \cdot sec^{-1}$)
La	$\sim 5.10^{-11}$ (10)
Fe	$\sim 5.10^{-12}$ (10)
O	$\sim 2.10^{-11}$ (11)

structure. In the whole reduction process, only the *B* metallic lattice, which in the normal perovskite constitutes a simple cubic sublattice, remains fixed and is responsible for the strong reflections characteristic of the perovskite substructure.

Although we do not have diffusion data for these species in $Ca_2LaFe_3O_8$, there exist some diffusion results typical of perovskite-like solids (Table II) which are in line with this reasoning. On the basis of these data, iron is the slowest among the three ions constituting $LaFeO_3$. In $Ca_2Fe_2O_5$ and $Ca_2LaFe_3O_8$ oxygen has to be even faster because the tunnels along [110] referred to above. Also La, and presumably also Ca, will move somewhat faster in those solids since the oxygen sublattice is not nearly as complete as in $LaFeO_3$.

Moreover Ca and La should have different diffusion rates if only because they are differently charged. Kinetic gradients may then be produced of both Ca and La facilitating the formation of "compositional gradients" with respect to those cations (i.e., microdomains of $Ca_2Fe_2O_5$ and of $LaFeO_3$). Reasonably enough, iron, being the slowest, is the material forming the skeleton which remains "rigid" all over the process.

This type of reasoning is in line with the ideas (*12*) of considering the crystal structure of some compounds as derived from metallic arrays with anions inserted, of which the fluorite-type structure is archetypal with F^- ions inserted in a face-centered cubic Ca array. In this case, a perovskite-like case, an anion, O^{2-} and a cation Ca^{2+} or La^{3+} are inserted in an iron simple cubic framework.

Considering the stoichiometry of the above Eq. (2) 1 mole of $Ca_2LaFe_3O_8$ gives 1 mole of $LaFeO_3$ and another of $Ca_2Fe_2O_5$ but as each of these is formed in three types of microdomains each microdomain of the original material originates, at least, six microdomains of the product phases which are necessarily smaller than the original one. This explains the extremely disordered texture of Fig. 6; however, each of these microdomains is an ordered unit of the corresponding phase. No correlation appears to exist, however, among the different units. The final state, as observed on Fig. 8, is formed by bigger domains produced in a recrystallization process. It is clear that microdomains are the essential characteristic of these oxido-reduction processes of $Ca_2LaFe_3O_8$.

The present results show then that under appropriate conditions a nonstoichiometric phase, $Ca_2LaFe_3O_{8.235}$, becomes unstable, but instead of reducing down to the stoichiometric composition $Ca_2LaFe_3O_8$, it decomposes in two more stable phases, $Ca_2Fe_2O_5$ and $LaFeO_3$. This behavior, which is typical of alloys (*13*) and minerals (*14*) where it is usually called exsolution, is also frequent in the world of synthetic solids since it is just a reflection of the thermodynamic stability of the three phases. If we were to consider the $Ca_2LaFe_3O_{8.235}$ solid as an "oxygen defective perovskite," under certain circumstances, i.e., under the electron beam, it decomposes to a phase "richer" in "oxygen defects," i.e., $Ca_2Fe_2O_5$ and another one "poorer" in "oxygen defects," i.e., $LaFeO_3$. However, it is to be stressed that considering $Ca_2Fe_2O_5$ as an oxygen deficient perovskite is only a for-

mal geometrical description. No oxygen *defects* are present in $Ca_2Fe_2O_5$, there are just unoccupied positions in the *Pcmn* space group.

As for the mechanism two kinds of phase transformation are usually distinguished, nucleation plus growth and spinodal (*15*), and they differ in the spatial extent of the resulting phases at the beginning of the process. Although it is not usually obvious to distinguish between these cases, the fact that we can *always* observe, from the very beginning of the decomposition, the diffraction patterns of both parent and products would seem to imply that the nucleation and growth process is predominant here. In this way the differences observed among Figs. 4–6 are just a reflection of the extent of the decomposition up to the instant in which the picture is taken.

It is worth recalling that, as we have recently discussed (*3, 16*), $Ca_2Fe_2O_5$ does not form microdomains under normal pressure oxidation conditions. However, it does so, in the presence of some lanthanum substituting for calcium. It is therefore not surprising that, in the present case, where both La and Ca have to diffuse all over the crystal, some La will be present in the brownmillerite-type domains. Consequently, some Ca is likely to be present in the $LaFeO_3$-type domains.

Acknowledgments

We thank Professor P. Hagenmuller for encouragement, Dr. Hj. Matzke for some of the diffusion data, and Dr. J. C. Grenier for providing the samples. We also thank L. Puebla and A. García for technical assistance.

References

1. M. A. Alario-Franco, M. J. R. Henche, M. Vallet-Regí, J. M. González-Calbet, J. C. Grenier, A. Wattiaux, and P. Hagenmuller, *J. Solid State Chem.* **46,** 23 (1983).
2. J. M. González-Calbet, M. Vallet-Regí, M. A. Alario-Franco, and J. C. Grenier, *Mater. Res. Bull.* **18,** 285 (1983).
3. M. A. Alario-Franco, J. M. González-Calbet, M. Vallet-Regí, and J. C. Grenier, *J. Solid State Chem.* **49,** 219 (1983).
4. M. Vallet-Regí, J. M. González-Calbet, M. A. Alario-Franco, J. C. Grenier, and P. Hagenmuller, *J. Solid State Chem.* **55,** 251 (1984).
5. J. C. Grenier, I. Darriet, M. Pouchard, and P. Hagenmuller, *Mater. Res. Bull.* **11,** 1219 (1976).
6. M. Marezio and P. Dernier, *Mater. Res. Bull.* **6,** 23 (1971).
7. E. F. Bertaut, L. Blum, and A. Sagnieres, *Acta Crystallogr.* **12,** 149 (1959). A. A. Colville, *Acta Crystallogr. B* **26,** 1469 (1970). J. Berggren, *Acta Chem. Scand.* **25**(*10*), 3616 (1971).
8. M. A. O'Keefe and P. Buseck, *Trans. Amer. Crystallogr. Assoc.* **15,** 27 (1979).
9. D. A. Wadsley, *in* "Non-stoichiometric Compounds" (L. Mandelcorn, Ed.), Academic Press, New York (1964).
10. I. E. Shimanovich. M. M. Paulyuchenko, B. O. Filonov, and S. A. Prokudina, *Vesti Akad. Navuk B SSR, Ser. Khim. Navuc,* No. 6, 61 (1969).
11. T. Ishigaki, S. Yamauchi, J. Mizusaki, K. Fueki, H. Naito, and T. Adachi, *J. Solid State Chem.* **55,** 50 (1984).
12. M. O'Keeffe, and B. G. Hyde, *Acta Crystallogr. B* **33,** 3802 (1977).
13. P. E. Champness and G. W. Lorimer, *in* "Electron Microscopy in Mineralogy" (H. R. Wenk, Ed.), Chapt. 4, Springer-Verlag, New York (1976).
14. J. E. Hilliard, "Phase Transformations," Amer. Soc. Met., pp. 497–560, Detroit (1970).
15. J. W. Cahn, *Acta Metall.* **9,** 795 (1961); *Trans. AIME* **242,** 166 (1968).
16. M. Vallet-Regí, J. M. González-Calbet, J. Verde, and M. A. Alario-Franco, *J. Solid State Chem.* **57,** 197 (1985).